Clim. Past Discuss., 11, 489–519, 2015
www.clim-past-discuss.net/11/489/2015/
doi:10.5194/cpd-11-489-2015

Climate of the Past
Discussions
Open Access

1200 years of warm-season temperature variability in central Fennoscandia inferred from tree-ring density

P. Zhang[1], H. W. Linderholm[1], B. E. Gunnarson[2], J. Björklund[3], and D. Chen[1]

[1]Regional Climate Group, Department of Earth Sciences, University of Gothenburg, Gothenburg, Sweden
[2]Bert Bolin Centre for Climate Research, Department of Physical Geography and Quaternary Geology, Stockholm University, Stockholm, Sweden
[3]Swiss Federal Research Institute WSL, Birmensdorf, Switzerland

Received: 12 January 2015 – Accepted: 27 January 2015 – Published: 19 February 2015

Correspondence to: P. Zhang (peng.zhang@gvc.gu.se)

Published by Copernicus Publications on behalf of the European Geosciences Union.

Abstract

An improved and extended *Pinus sylvestris L.* (Scots Pine) tree-ring maximum density (MXD) chronology from the central Scandinavian Mountains was used to reconstruct warm-season (April–September) temperature back to 850 CE. Due to systematic bias from differences in elevation (or local environment) of the samples through time, the data was "mean adjusted'. The new reconstruction, called C-Scan, was based on the RSFi standardisation method to preserve mid- and long-term climate variability. C-Scan, explaining more than 50 % of the warm-season temperature variance in a large area of Central Fennoscandia, agrees with the general profile of Northern Hemisphere temperature evolution during the last 12 centuries, supporting the occurrences of a Medieval Climate Anomaly (MCA) around 1009–1108 CE and a Little Ice Age (LIA) ca 1550–1900 CE in Central Fennoscandia. C-scan suggests a later onset of LIA and a larger cooling trend during 1000–1900 CE than previous MXD based reconstructions from Northern Fennoscandia. Moreover, during the last 1200 years, the coldest period was found in the late 17th–19th centuries with the coldest decades being centered on 1600 CE, and the warmest 100 years occurring in the most recent century.

1 Introduction

Fennoscandia has a strong tradition in dendrochronology, and its large tracts of boreal forest make the region well suited for the development of tree-ring chronologies that extend back several thousands of years (Linderholm et al., 2010). In addition to the well-known multi-millennial tree-ring width chronologies from Torneträsk (Grudd et al., 2002), Finnish Lapland (Helama et al., 2002) and Jämtland (Gunnarson et al., 2003), several millennium long temperature-sensitive tree-ring datasets were collected within the European Union funded "Millennium" project (McCarroll et al., 2013). However, these are all, except for Jämtland and Mora (822 year Blue intensity, Graham et al., 2011), located in northernmost Fennoscandia. It has been shown that in or-

CPD
11, 489–519, 2015

der to better represent Fennoscandian warm-season temperature variability, data from more southern locations are needed (Linderholm et al., 2014a). Thus, getting high-quality data from the central parts of Fennoscandia is needed. Helama et al. (2014) reconstructed May–September temperature variability in southern Finland for the last millennium using maximum latewood density (MXD) data. In Sweden, presently the southernmost site to provide a robust temperature signal from tree-ring MXD data is the central Scandinavian Mountains, in the province of Jämtland, where Gunnarson et al. (2011, henceforth G11) reconstructed 900 years of warm-season temperatures. Because of the relatively southerly location, Jämtland is considered a key location for paleotemperature studies in Scandinavia. Not only can it function as a link between chronologies in northern Fennoscandia and those in continental Europe (Gunnarson et al., 2011), but also the closeness to the North Atlantic makes it a suitable place to investigate long-term associations between marine and terrestrial climate variability (e.g., Cunningham et al., 2013).

At northern high latitudes, MXD and the newly developed ΔDensity parameter are the most powerful warm-season temperature tree-ring proxies, compared to tree-ring widths (Briffa et al., 2002; Björklund et al., 2014). The longest MXD records are found in northernmost Fennoscandia (see McCarroll et al., 2013; Melvin et al., 2013; Esper et al., 2012). These chronologies are exclusively based on material with known temperature sensitive provenience, from living trees, dry deadwood and, in the case of N-Scan, subfossil wood (Esper et al., 2012). The G11, however, also included historical material (tree-ring samples from historical buildings). The historical samples were collected from buildings in Jämtland in the 1980s, as a part of a grand sampling strategy to focus on a dense tree-ring density network from cool moist regions (Schweingruber et al., 1990). Due to the limited number of deadwood samples from the studied area in the Scandinavian Mountains, the historical samples, belonging to the period between 1107 and 1827 CE (with a gap between 1292–1315 CE), made up the major part of the G11 reconstruction. Since the geographical origin of the historical samples is unclear, it was difficult to fully assess the validity of the interpreted temperature signal. Compar-

CPD
11, 489–519, 2015

ing G11 to the Fennoscandian June–August summer temperature reconstruction from Gouirand et al. (2008), a coherency was found between AD 1300 and 1900, but G11 showed a stronger warming between AD 1100 and 1300. One explanation for the differences between the two records could be regional differences in the temporal evolution of warm-season temperatures in central and northern Scandinavia (Gunnarson et al., 2011). For instance, Gunnarson and Linderholm (2002) suggested that the Medieval Climate Anomaly (MCA, 10th–13th CE, Grove and Switsur, 1994) was of shorter duration but more pronounced in the central Scandinavian Mountains compared to Northern Scandinavia. Another reason for this apparent difference in late-MCA temperatures could be that the tree-ring samples collected from the historical buildings do not truly reflect summer temperature variability in the mountains due to their likely low-elevation origins.

To overcome this uncertainty, we developed a warm-season (April through September) temperature reconstruction for the last 1200 years based exclusively on Scots pine samples from sites close to the current altitude timber-line in a relatively limited area. Since there was an elevational difference in the temporal distribution of the samples, we also considered the impact of the temperature lapse rate and local environment on MXD values, and corrected the MXD values according to the mean-adjustment method (Zhang et al., 2015). Furthermore, the traditional RCS (regional curve standardisation) method (Briffa et al., 1992) was compared with the new RSFi (regional curve adjusted individual signal-free approach) method (Björklund et al., 2014) when developing the chronology.

2 Data and method

2.1 Study area

The province of Jämtland is located in the westernmost part of central Sweden (Fig. 1). The region belongs to the Northern Boreal zone, and the study area is situated just

CPD
11, 489–519, 2015

east of the Scandinavian Mountains main divide. The main topography ranges from 800 to 1000 m a.s.l., but scattered alpine massifs to the south reach approximately 1700 m a.s.l. There is a distinct climate gradient in the area. East of the Scandinavian Mountains, climate can be described as semi-continental. However, the proximity to the Norwegian Sea, lack of high mountains in the west, and the east–west oriented valleys allow moist air to be advected from the ocean, providing an oceanic influence to the area. Consequently, the study area is located in a border zone between oceanic and continental climates. On short timescales, summer climate of this particular region is influenced by the atmospheric circulation, mainly the North Atlantic Oscillation (NAO) (Chen and Hellström, 1999), while it is affected by North Atlantic sea-surface temperature (SST) on longer timescales (Rodwell et al., 1999; Rodwell and Folland, 2002).

Glacial deposits dominate the area, mainly till but also glacifluvial deposits, peatlands and small areas of lacustrine sediments (Lundqvist, 1969). The forested parts in the central Scandinavian Mountains are dominated by *Pinus sylvestris L.* (Scots Pine), *Picea abies* (Norway spruce) and *Betula pubescens* (Mountain birch). Although large-scale forestry have been carried out in most parts of the county, the human impact on trees growing close to the tree line is limited, which is valuable in tree-ring based climate reconstructions (Gunnarson et al., 2012). Due to the short and cool summers, dry deadwood can be preserved for more than 1000 years (Linderholm et al., 2014b). Moreover, large amounts of subfossil wood from hundreds to thousands of years ago can be found in small mountain lakes (see Gunnarson, 2008).

2.2 Tree-ring data

The tree-ring data used in this study came from 8 sites (Table 1). As shown in Fig. 1, they are all at a close distance, but differ in elevation and local environment. From the small peak Furuberget, 142 samples were collected close to the top at ca. 650 m a.s.l. in an open pine forest with limited competition between trees. Pine trees grow on a relatively flat area covered by a thick vegetation layer with

CPD
11, 489–519, 2015
1200 years of warm-season temperature variability
P. Zhang et al.

woody dwarf shrubs and mosses. The area is characterized by thin till and glacifluvial soils. 35 of these samples were included in G11 (Table 1). In addition, pine samples were collected at different elevations on Mount Håckervalen from the present tree line (at around 650 m a.s.l.) up to 800 m a.s.l., described in detail in Linderholm et al. (2014b). At both sites living trees and dry deadwood were sampled. Samples preserved in lakes (so called subfossil wood) were included from the lakes Lill-Rörtjärnen, Östra Helgtjärnen and Jens-Perstjärnen, previously described in Gunnarson (2008). The historical tree-ring data, collected from historical buildings in the province was downloaded from the International Tree-Ring Data Bank (ONLINE RESOURCE: https://www.ncdc.noaa.gov/paleo/study/4447).

The new MXD measurements (Table 1) were produced using an ITRAX Wood scanner from Cox Analytic System (http://www.coxsys.se). For further information of the ITRAX settings, see Gunnarson et al. (2011). The historical samples was collected by Schweingruber et al. in the 1970s (Schweingruber et al., 1991) and the MXD measurements was obtained using the DENDRO2003 x-ray instrumentation from Walesh Electronic (http://www.walesch.ch/). All samples were prepared according to standard dendrochronological techniques (Schweingruber et al., 1978).

It was previously found that in the studied region, the absolute MXD values differ with respect to elevation, which is likely due to the temperature lapse rate (Zhang et al., 2015). In short, the absolute MXD values at higher elevation are systematically lower than those from lower elevation. Moreover, the elevation effect on the absolute MXD values is larger than the effect of temperature differences between warm (MCA) and cold (Little Ice Age, LIA, 14th–19th centuries Grove, 2001) periods. Thus, an average chronology with a heterogeneous elevational sample distribution through time, e.g. older samples are found only at progressively higher elevations, will contain systematic differences in their means during different periods. If not attended to this may introduce biases to an average chronology, both in terms of the high-resolution variability (annual to decadal) and the long term trend. It is evident from Fig. 2, that there are periods when the samples from different elevations do not overlap in time, e.g. 1550–1800 (no samples from Håckervalen-top and Furuberget 1 overlap.). To overcome this problem, we adjusted the mean MXD value from the different elevations to have the same mean during a period of overlap. The mean MXD value of the Furuberget 1 samples, covering 1300–1550, was used as a reference to adjust the samples from other groups except for the sites Håckervalen and Furuberget 2 (samples from these two groups do not cover 1300–1550). A constant was added to or subtracted from each sample of a group in order to force the samples to have the same mean MXD value as the reference. Since the living trees from Håckervalen (650 m) and Furuberget 2 have the same elevation as Furuberget 1, and both of the sites do not have significantly different mean MXD values with the Furuberget 1 samples during 1800–2000, we did not adjust the samples from these two sites. We chose Furuberget 1 as a reference site, because the Furuberget 1 samples had a high sample replication and a wide temporal coverage. Other ways to deal with this problem is to standardise the samples site-by-site (or group-by-group) rather than adjusting the mean value of each group of samples. However, this method works well when all groups have the same or similar temporal distribution.

2.3 Standardisation method and chronology building

If tree-ring data is going to be used to attain reliable climate information, it is pertinent to remove as much non-climatic information as possible before building a chronology from the individual tree-ring series (Fritts, 1976). The non-climatological growth expression is usually represented with a least square fitted negative exponential function, polynomial or spline (Fritts, 1976; Cook and Peters, 1981), and subtracted or divided from each raw tree-ring measurement to obtain indices used for chronology building, in a process termed standardisation. This approach is widely used, but it severely limits the attained low-frequency variability in long chronologies (with several generations of trees), because all indices have similar averages, referred to as the “segment length curse” (Cook et al., 1995; Briffa et al., 1996).

CPD
11, 489–519, 2015

This limitation can be overcome by quantifying the non-climatological growth expression for an entire population as an average of the growth of all samples aligned by cambial age, which then can be represented by a single mathematical function. Subsequently this function is subtracted from or divided by each individual tree-ring measurement, where this process is called Regional Curve Standardisation (RCS Briffa et al., 1992). However, by using one single function for all tree-ring series, less unwanted mid-frequency variability is removed in the attempt to preserve the low-frequency (> segment length) variability (Melvin, 2004), along with possible trend distortion as described in Melvin and Briffa (2008). Alternatively, the non-climatological expression in tree-ring data can be quantified with the signal-free (SF) approach to standardisation, described in Melvin and Briffa (2008), either on individual trees or on an average of all trees (RCS). Using SF RCS can alleviate possible trend distortions, but limited noise from stand competition etc. is removed.

By using the SF individual fitting approach and at the same time letting the derived functions to have a similar mean as their respective cambial age segment of the regional curve (RC) before subtraction into indices, stand competition etc. can also be addressed without losing the long timescale component (Björklund et al., 2013). This approach was termed RSFi (ibid.). We compared chronologies resulting from the above described standardisation methods: classic RCS, SF RCS and RSFi, where the chronology used for reconstruction was derived with RSFi. The expressed population signal (EPS) criterion was used to evaluate the robustness of the chronology. An EPS value represents the percentage of the variance in the hypothetical population signal in the region that is accounted for by the chronology, where EPS values greater than 0.85 are generally regarded as sufficient (Wigley et al., 1984).

2.4 Instrumental data

Monthly temperature data from the closest meteorological station, Duved (400 m a.s.l., 63.38° N, 12.93° E), was used to assess the temperature signal reflected by the chronology. Since the data from this station only cover the period of 1911–1979,

CPD
11, 489–519, 2015

we extended the data back to 1890 and up to 2011 by using linear regression on monthly temperature data from an adjacent station: Östersund (376 m a.s.l., 63.20° N, 14.49° E). A linear regression was done to relate mean temperature of each month from Östersund station to that from Duved station. Data from Östersund explain on average 91.5 % of the interannual variance in Duved monthly temperature (based on the overlapping period 1911–1979). The temperature data from Östersund came from two sources: the Nordklim data base (1890–2001) (Tuomenvirta et al., 2001), and Swedish Meteorological and Hydrological Institute (SMHI, 2001–2011). The locations of Duved and Östersund stations are shown in Fig. 1.

3 Warm-season temperatures reconstruction

3.1 Comparing MXD samples of different origin

After having adjusted the mean value of each group of samples, we compared the two chronologies based on the “in situ” and historical samples respectively. Three standardisation methods were applied to build the chronologies. Figure 3 shows a comparison of the z scored (based on 1700–1800) historical-sample chronology (HSC, blue curves) and the ”in situ”- chronology (ISC, black curves) produced by the signal-free RCS (Fig. 3a), negative exponential function standardisation (Fig. 3b), and RSFi standardisation (Fig. 3c) methods. Clearly, the same features can be observed regardless of the standardisation methods: (1) on multidecadal scales, the HSC agrees quite well with ISC between 1300 and 1800 CE, but the HSC displays a smaller variance than the ISC; (2) between 1100 and 1300 CE there is a notable disagreement between HSC and ISC. On interannual scale (based on 1st difference chronologies), the HSC can explain 34 % variance of ISC during 1100–1300 CE, and explain 62 % of the variance during 1300–1800 CE. Moreover, it should be noted that the 50 year-window EPS values fall below 0.85 for both chronologies during the 1160–1220 CE period. We tested boosting the ISC with the historical samples during 1100–1300. The statistic results show that the EPS of the boosted chronology during 1160–1210 is still below 0.85, and the EPS during 1225–1265 is even smaller than before boosting. Only the EPS during 1212–1222 changed from below 0.85 to above 0.85. Consequently, there was no significant improvement of the robustness of the ISC during 1100–1300 CE after including the historical samples.

3.2 The influence of standardisation method

At present, RCS and signal-free RCS are the most favoured standardisation methods when building chronologies intended to have their long-term variability preserved. We examined the performances of the two RCS methods and the RSFi method. As shown in Fig. 4, the difference among the three differently standardised chronologies is mainly reflected in the multi-decadal variability. The chronologies produced by the both RCS methods are in very good agreement on multi-decadal timescales. Although the RSFi chronology shows a similar evolution as the RCS ones, it is obvious that they differ in some periods. In general, the RSFi chronology suggests slightly warmer conditions than the RCS based ones, especially pronounced during the late half of LIA. It is difficult to firmly state which one of the chronologies is closer to actual temperatures, but we argue that there is a benefit in using individual signal-free curves (the RSFi method) rather than a common regional signal-free curve (the RCS methods), since this procedure has a better potential to remove unwanted noise (e.g. related to stand dynamics) on tree level. Consequently, we opted for the RSFi chronology for the reconstruction.

3.3 Climate signal in the new chronology

We compared the new chronology with the instrumental monthly mean temperatures constructed for the Duved meteorological station during the period 1890–2011. Figure 5a shows that the new chronology has a significant positive correlation (at $p < 0.01$ level) with individual monthly mean temperatures in April through September, and the highest correlation was found with mean April–September temperature ($r = 0.77$).

Therefore, we decided to reconstruct the April–September mean temperature (henceforth referred to as warm-season temperature). The reconstructed and observed warm-season temperatures for the 1890–2011 period show a good agreement on interanual to multidecadal timescales (Fig. 5c), and the new MXD reconstruction explains approximately 59 % of the variance in the instrumental data (Fig. 5b).

3.4 The new reconstruction

In order to test the temporal stability of the MXD vs. observation when creating a model to reconstruct warm-season temperature back in time, we divided the instrumental period into two parts: 1890–1950 and 1951–2011, with the first part for calibration and the second part for verification. Then, we switched the calibration and verification periods, and repeated the same exercise. The calibration and verification statistics are shown in Table 2. The reduction of error statistic (RE) has a possible range of $-\infty$ to 1, and an RE of 1 can be achieved only if the prediction residuals equal zero. Zero is commonly used as a threshold, and the positive RE values in the both calibration periods suggests that our reconstruction has some skill (Table 2). Similar to RE, coefficient of efficiency (CE) is a measure to evaluate the model under the validation period. Values close to zero or negative suggests that the reconstruction is no better than the mean, whereas positive values indicate the strength and temporal stability of the reconstruction.

We evaluated the spatial representativeness of the new warm-season temperature reconstruction by correlating it with the CRU TS3.22 $0.5^{\circ} \times 0.5^{\circ}$ gridded warm-season temperature (Harris et al., 2014) for the period 1901–2011. The field correlation maps were plotted using the "KNMI climate explorer" (Royal Netherlands meteorological Institute; http://climexp.knmi.nl; Van Oldenborgh et al., 2009). We also compared the field correlation of observed warm-season temperature. As expected, Fig. 6 shows that the new reconstruction (Fig. 6a) captures a large part of the patterns from the observations (Fig. 6b). The reconstruction represents the warm-season temperature variation with correlations above 0.71 across much of Central Fennoscandia, which validates the good spatial representativeness of our reconstruction.

CPD
11, 489–519, 2015

4 Discussion

4.1 Central Fennoscandian warm-season temperature evolution

Figure 7 shows the reconstructed warm-season temperature of Central Fennoscandian, henceforth C-Scan, during the past 1200 years. C-Scan displays a cooling trend between 850 and 1800 CE, followed by a sharp temperature increase after the mid-19th century. In order to look at the C-Scan temperature evolution in more detail, we picked out the coldest and warmest periods (10, 30 and 100 years of mean temperatures respectively) during the last 1200 years (Fig. 7). The late 17th century to early 19th century was the coldest long-term period during the past 1200 years, and that the coldest 100 year-period appeared during the 19th century. Both the coldest 10 and 30 year periods appeared during the 17th century. The warmest 100 years coincides with the most recent 100 years, which is consistent with the anthropogenic warming period (Stocker et al., 2013). However, the warmest 10 and 30 year periods were found in the 13th century. Comparing the MCA with the current warming period showed that the warmest 100 year period during the MCA was 0.1 °C cooler than the 20th century. The warmest 10 and 30 year periods during the 20th century were 0.2 and 0.1 °C cooler respectively than those during the 13th century. Despite low sample depth, the warmest 10 and 30 year periods have 51 year EPS values above 0.85.

4.2 The influence on MXD of elevation differences

To highlight the application of mean-adjusted data in our reconstruction, we compared reconstructions based on mean-adjusted and unadjusted samples. As shown in Fig. 8, the reconstruction based on unadjusted samples (blue curve) yields a 0.4 °C lower average warm-season temperature during the period 850–1200 CE compared to the mean-adjusted reconstruction (black curve). Moreover, the long-term trend before the onset of the twentieth century clearly differs between the two, where the cooling trend in the mean-adjusted data is turned to a warming trend in the unadjusted. Consequently, a reconstruction based on unadjusted data would indicate that warm-season temperature in 850–1200 CE, roughly corresponding to the MCA, would be about 0.3 °C cooler than the subsequent four centuries (1201–1600 CE). This is quite contradictory to indications from other paleoclimate data for Fennoscandia (e.g., Esper et al., 2012; McCarroll et al., 2013; Melvin et al., 2013; Helama et al., 2014), as well as for the whole Northern Hemisphere.

Previous ways of dealing with samples of different origin (living trees, subfossil and historical wood), have used separate RCS curves for each type of samples (e.g., Gunnarson et al., 2011), but the prerequisite is that samples of different origin are from the same periods, or at least have a large overlap, so that any differences in long-term trend are to a large extent cancelled out when averaging. Given that we did have some overlap between our different data, we could have used the "separate RCS curves" method. However, although this method produces a similar reconstruction after the mid-13th century, it does deliver a mean temperature for 850–900 and 1150–1250 CE that is 0.2 °C lower than that by our method. Therefore, we choose to use of the mean-adjustment method.

4.3 Comparing C-Scan with Northern Hemisphere temperature pattern and Northern Fennoscandia MXD reconstruction

To set our new reconstruction in a wider context, we compared it with the Northern Hemisphere temperature patterns based on multi-proxy records (Ljungqvist et al., 2012). Our new reconstruction shows an agreement with the general profile of Northern Hemisphere temperature evolution during the last 12 centuries, supporting the occurrences of a MCA and LIA in Central Fennoscandia. The hemisphere scale temperature patterns shows that, despite differences in the onset of MCA or LIA phases regionally, the Northern Hemisphere generally experience a relative warm period during 800–1300 CE and a relative cold period during 1300–1900 CE, and followed by an intensive warming period after 1900 CE. However, there are some aspects where our reconstruction shows differences. One such aspect is that the warmest century during MCA in our reconstruction occurred during the 11th century, while the Northern Hemisphere temperature peak is found in the 10th century. Another aspect is that the cooling from MCA to the LIA seems to happen at a stable rate on the hemisphere scale, while our reconstruction shows a weak cooling during the transition period from the MCA to the LIA (1300–1500 CE), followed by an intensive cooling during the 16th century when central Scandinavia enter into a 300 year cold period. Globally, continental-scale temperature has shown a regional difference in temporal evolution during the last two millennia under natural forcings conditions (Ahmed et al., 2013). Thus, the lag of the warmest century during MCA and the late onset of LIA in central Fennoscandia can be explained by the regional temperature evolution. However, considering the late onset of LIA, our reconstruction seems more similar with the temperature evolution in North America and Australia rather than Arctic, Europe and Asia.

Zooming in to Fennoscandia, we compared C-Scan to the MXD derived summer temperature reconstruction from northern Fennoscandia (N-Scan, Esper et al., 2012). From Fig. 10a, it is clear that although our new reconstruction agrees well with the long-term cooling up until 1900, discussed by Esper et al. (2012), some obvious differences can be noted. The long term cooling trend is slightly more pronounced in C-Scan (0.48 °C per 1000 years over the period of 1000–1900 CE, compared to 0.36 °C in N-Scan). Moreover, C-Scan infers cooler temperatures than N-Scan during two longer periods roughly corresponding to the early half of MCA (900–1100 CE) and late half of LIA (1550–1900 CE). Also, the two records seem to be offset between 850 and 1300. However, it should be noted that the two reconstructions agree quite well on interannual timescale, except for the period 1230–1280. The more or less anti-phase behaviour in C-Scan between 1150 and 1250 is likely due to the drop in sample sizes in C-Scan at that time. Comparing the 101 year running R-bar in the two MXD series (after age-dependent spline detrending) of the two reconstructions shows that the mean running R-bar values are 0.45 and 0.46 for C-Scan (65 series (trees) covering 850–1406 CE) and N-Scan samples (50 series (trees) covering 850–1404 CE) respectively. This indicates that both reconstructions reflect common signals of their respective sample populations during the period of disagreement.

When compared with the 1500 year long MXD based May–August temperature reconstruction from Torneträsk (Melvin et al., 2013), C-Scan infers slightly warmer temperatures during 1200–1700 CE, and in general differs from the Torneträsk reconstruction at multi-decadal to century timescales during 1100–1900 CE. However, they are in quite good agreement on interannual timescale. The running R-bar curves also indicate the both reconstructions reflect common signals of their respective sample population.

Despite the proximity, C-scan shows some different features from the temperature evolution in Northern Fennoscandia, such as a later onset of the LIA. This possibly indicates that the warm-season temperature evolution differs also within Fennoscandia. Under anthropogenic forcing conditions, global temperature shows a significant warming trend. However, the warming trends can be different in their magnitudes in different regions, due to differnces in regional settings and processes. In addition to the different heat capacity between continent and ocean and the snow-ice feedback, other physical mechanisms behind this should be well addressed in order to project the future regional temperature. To well address this issue, more high resolution regional temperature reconstructions are needed.

5 Conclusions

An updated and extended version of the Jämtland MXD chronology was used to reconstruct the warm-season temperature (April–September) evolution in Central Fennoscandia for the period 850–2011 CE. Due to the fact that the samples come from different elevations, the new reconstruction, called C-Scan, was based on mean-adjusted data subsequently standardised with the RSFi method. Our new reconstruction suggests a MCA during ca 1009 to 1108, followed by a transition period before the onset of the Little Ice Age proper in the mid-16th century. The cooling trend (−0.48 °C per 1000 years) during 1000–1900 is greater than that inferred from northern

CPD
11, 489–519, 2015

Fennoscandia (Esper et al., 2012). During the last 1200 years, the late 17th century to early 19th century was the coldest period in central Fennoscandia, and the warmest 100 years occurred during the most recent century in central Fennoscandia, and the coldest decades occurred around 1600 CE.

Acknowledgements. We acknowledge the County Administrative Boards of Jämtland for giving permissions to conduct dendrochronological sampling, and Mauricio Fuentes, Petter Stridbeck, Riikka Salo, Emad Farahat and Eva Rocha for their help in the field. We also thank Laura McGlynn and Håkan Grudd for assistance in the MXD measurements and Andrea Seim for helping out with GIS. This work was supported by Grants from the two Swedish research councils (Vetenskapsrådet and Formas, Grants to Hans Linderholm) and the Royal Swedish Academy of Sciences (Kungl. Vetenskapsakademien, grant to Peng Zhang). This research contributes to the strategic research areas Modelling the Regional and Global Earth system (MERGE), and Biodiversity and Ecosystem services in a Changing Climate (BECC) and to the PAGES2K initiative. This is contribution # 33 from the Sino-Swedish Centre for Tree-Ring Research (SISTRR).

References

Ahmed, M., Anchukaitis, K., Buckley, B. M., Braida, M., Borgaonkar, H. P., Asrat, A., Cook, E. R., Büntgen, U., Chase, B. M., and Christie, D. A.: PAGE 2k Consortium: Continental-scale temperature variability during the past two millennia, Nat. Geosci., 6, 339–346, 2013. 502

Björklund, J. A., Gunnarson, B. E., Krusic, P. J., Grudd, H., Josefsson, T., Östlund, L., and Linderholm, H. W.: Advances towards improved low-frequency tree-ring reconstructions, using an updated Pinus sylvestris L. MXD network from the Scandinavian Mountains, Theor. Appl. Climatol., 113, 697–710, 2013. 496

Björklund, J. A., Gunnarson, B. E., Seftigen, K., Esper, J., and Linderholm, H. W.: Blue intensity and density from northern Fennoscandian tree rings, exploring the potential to improve summer temperature reconstructions with earlywood information, Clim. Past, 10, 877–885, doi:10.5194/cp-10-877-2014, 2014. 491, 492

Briffa, K. R., Jones, P. D., Bartholin, T. S., Eckstein, D., Schweingruber, F. H., Karlen, W., Zetterberg, P., and Eronen, M.: Fennoscandian summers from AD 500: temperature changes on short and long timescales, Clim. Dynam., 7, 111–119, 1992. 492, 496

CPD
11, 489–519, 2015

Briffa, K. R., Jones, P. D., Schweingruber, F. H., Karlén, W., and Shiyatov, S. G.: Tree-Ring Variables as Proxy-Climate Indicators: Problems with Low-Frequency Signals, Springer, 9–41, 1996. 495

Briffa, K. R., Osborn, T. J., Schweingruber, F. H., Jones, P. D., Shiyatov, S. G., and Vaganov, E. A.: Tree-ring width and density data around the Northern Hemisphere: Part 1, local and regional climate signals, The Holocene, 12, 737–757, 2002. 491

Chen, D., and Hellström, C.: The influence of the North Atlantic Oscillation on the regional temperature variability in Sweden: spatial and temporal variations, Tellus A, 51, 505–516, 1999. 493

Cook, E. R. and Peters, K.: The Smoothing Spline: A New Approach to Standardizing Forest Interior Tree-Ring width Series for Dendroclimatic Studies, 1981. 495

Cook, E. R., Briffa, K. R., Meko, D. M., Graybill, D. A., and Funkhouser, G.: The "segment length curse" in long tree-ring chronology development for palaeoclimatic studies, The Holocene, 5, 229–237, 1995. 495

Cunningham, L. K., Austin, W. E., Knudsen, K. L., Eiríksson, J., Scourse, J. D., Wanamaker, A. D., Butler, P. G., Cage, A. G., Richter, T., and Husum, K.: Reconstructions of surface ocean conditions from the northeast Atlantic and Nordic seas during the last millennium, The Holocene, 23, 921–935, 2013. 491

Esper, J., Frank, D. C., Timonen, M., Zorita, E., Wilson, R. J., Luterbacher, J., Holzkämper, S., Fischer, N., Wagner, S., and Nievergelt, D.: Orbital forcing of tree-ring data, Nature Climate Change, 2, 862–866, 2012. 491, 501, 502, 504, 519

Fritts, H.: Tree Rings and Climate, ACADEMIC PRESS INC. (LONDON) LTD, London, UK, 1976. 495

Gouirand, I., Linderholm, H. W., Moberg, A., and Wohlfarth, B.: On the spatiotemporal characteristics of Fennoscandian tree-ring based summer temperature reconstructions, Theor. Appl. Climatol., 91, 1–25, 2008. 492

Graham, R., Robertson, I., McCarroll, D., Loader, N., Grudd, H., and Gunnarson, B.: Blue Intensity in Pinus sylvestris: application, validation and climatic sensitivity of a new palaeoclimate proxy for tree ring research, in: AGU Fall Meeting Abstracts, vol. 1, p. 1896, 9–41, 2011. 490

Grove, J. M.: The Initiation of the "Little Ice Age" in Regions Round the North Atlantic, Springer, 53–82, 2001. 494, 517

Grove, J. M. and Switsur, R.: Glacial geological evidence for the Medieval Warm Period, Climatic Change, 26, 143–169, 1994. 517

CPD
11, 489–519, 2015

1200 years of warm-season temperature variability

P. Zhang et al.

Grudd, H., Briffa, K. R., Karlén, W., Bartholin, T. S., Jones, P. D., and Kromer, B.: A 7400-year tree-ring chronology in northern Swedish Lapland: natural climatic variability expressed on annual to millennial timescales, The Holocene, 12, 657–665, 2002. 490

Gunnarson, B. E.: Temporal distribution pattern of subfossil pines in central Sweden: perspective on Holocene humidity fluctuations, The Holocene, 18, 569–577, 2008. 493, 494

Gunnarson, B. E. and Linderholm, H. W.: Low-frequency summer temperature variation in central Sweden since the tenth century inferred from tree rings, The Holocene, 12, 667–671, 2002. 492

Gunnarson, B. E., Borgmark, A., and Wastegård, S.: Holocene humidity fluctuations in Sweden inferred from dendrochronology and peat stratigraphy, Boreas, 32, 347–360, 2003. 490

Gunnarson, B. E., Linderholm, H. W., and Moberg, A.: Improving a tree-ring reconstruction from west-central Scandinavia: 900 years of warm-season temperatures, Clim. Dynam., 36, 97–108, 2011. 491, 492, 494, 501

Gunnarson, B. E., Josefsson, T., Linderholm, H. W., and Östlund, L.: Legacies of pre-industrial land use can bias modern tree-ring climate calibrations, Clim. Res., 53, 63–76, 2012. 493

Harris, I., Jones, P., Osborn, T., and Lister, D.: Updated high resolution grids of monthly climatic observations – the CRU TS3. 10 Dataset, Int. J. Climatol., 34, 623–642, 2014. 499

Helama, S., Lindholm, M., Timonen, M., Meriläinen, J., and Eronen, M.: The supra-long Scots pine tree-ring record for Finnish Lapland: Part 2, interannual to centennial variability in summer temperatures for 7500 years, The Holocene, 12, 681–687, 2002. 490

Helama, S., Vartiainen, M., Holopainen, J., Mäkelä, H. M., Kolström, T., and Meriläinen, J.: A palaeotemperature record for the Finnish Lakeland based on microdensitometric variations in tree rings, Geochronometria, 41, 265–277, 2014. 491, 501

Linderholm, H. W., Björklund, J. A., Seftigen, K., Gunnarson, B. E., Grudd, H., Jeong, J.-H., Drobyshev, I., and Liu, Y.: Dendroclimatology in Fennoscandia – from past accomplishments to future potential, Clim. Past, 6, 93–114, doi:10.5194/cp-6-93-2010, 2010. 490

Linderholm, H., Björklund, J., Seftigen, K., Gunnarson, B., and Fuentes, M.: Fennoscandia revisited: a spatially improved tree-ring reconstruction of summer temperatures for the last 900 years, Clim. Dynam., 1–15, doi:10.1007/s00382-014-2328-9, 2014a. 491

Linderholm, H. W., Zhang, P., Gunnarson, B. E., Björklund, J., Farahat, E., Fuentes, M., Rocha, E., Salo, R., Seftigen, K., and Stridbeck, P.: Growth dynamics of tree-line and lake-shore Scots pine (Pinus sylvestris L.) in the central Scandinavian Mountains dur-

ing the Medieval Climate Anomaly and the early Little Ice Age, Paleoecology, 2, 20, doi:10.3389/fevo.2014.00020, 2014b. 493, 494
Ljungqvist, F. C., Krusic, P. J., Brattström, G., and Sundqvist, H. S.: Northern Hemisphere temperature patterns in the last 12 centuries, Clim. Past, 8, 227–249, doi:10.5194/cp-8-227-2012, 2012. 501
Lundqvist, J.: Beskrivning till jordartskarta över Jämtlands län: 4 Karten. Kt, Sveriges Geologiska Undersökning, 1969. 493
McCarroll, D., Loader, N. J., Jalkanen, R., Gagen, M. H., Grudd, H., Gunnarson, B. E., Kirchhefer, A. J., Friedrich, M., Linderholm, H. W., and Lindholm, M.: A 1200-year multiproxy record of tree growth and summer temperature at the northern pine forest limit of Europe, The Holocene, 0, 1–14, 2013. 490, 491, 501
Melvin, T. M.: Historical Growth Rates and Changing Climatic Sensitivity of Boreal Conifers, University of East Anglia, Norwich, UK, 2004. 496
Melvin, T. M. and Briffa, K. R.: A “signal-free” approach to dendroclimatic standardisation, Dendrochronologia, 26, 71–86, 2008. 496
Melvin, T. M., Grudd, H., and Briffa, K. R.: Potential bias in “updating” tree-ring chronologies using regional curve standardisation: re-processing 1500 years of Torneträsk density and ring-width data, The Holocene, 23, 364–373, 2013. 491, 501, 503, 519
Rodwell, M. and Folland, C.: Atlantic air–sea interaction and seasonal predictability, Q. J. Roy. Meteor. Soc., 128, 1413–1443, 2002. 493
Rodwell, M., Rowell, D., and Folland, C.: Oceanic forcing of the wintertime North Atlantic Oscillation and European climate, Nature, 398, 320–323, 1999. 493
Schweingruber, F., Fritts, H., Bräker, O., Drew, L., and Schär, E.: The X-Ray Technique as Applied to Dendroclimatology, 1978. 494
Schweingruber, F., Kairiukstis, L., and Shiyatov, S.: Sample Selection, Methods of Dendrochronology: Applications in the Environmental Sciences, 23–35, 1990. 491
Schweingruber, F., Briffa, K., and Jones, P.: Yearly maps of summer temperatures in western Europe from AD 1750 to 1975 and western North America from 1600 to 1982, Vegetatio, 92, 5–71, 1991. 494
Stocker, T., Qin, D., Plattner, G., Tignor, M., Allen, S., Boschung, J., Nauels, A., Xia, Y., Bex, V., and Midgley, P.: IPCC, 2013: summary for policymakers, in: Climate Change 2013: The Physical Science Basis, Contribution of Working Group I to the Fifth Assessment Report of the

Intergovernmental Panel on Climate Change, Cambridge Univ. Press, Cambridge, UK, 3–29, 2013. 500

Tuomenvirta, H., Drebs, A., Førland, E., Tveito, O. E., Alexandersson, H., Laursen, E. V., and Jónsson, T.: Nordklim data set 1.0 description and illustrations, Tech. rep., DNMI Report, 2001. 497

van Oldenborgh, G. J., Drijfhout, S., van Ulden, A., Haarsma, R., Sterl, A., Severijns, C., Hazeleger, W., and Dijkstra, H.: Western Europe is warming much faster than expected, Clim. Past, 5, 1–12, doi:10.5194/cp-5-1-2009, 2009. 499

Wigley, T. M., Briffa, K. R., and Jones, P. D.: On the average value of correlated time series, with applications in dendroclimatology and hydrometeorology, J. Clim. Appl. Meteorol., 23, 201–213, 1984. 496

Zhang, P., Björklund, J., and Linderholm, H. W.: The influence of elevational differences in absolute maximum density values on regional climate reconstructions, in review, 2015. 492, 494

CPD
11, 489–519, 2015

1200 years of warm-season temperature variability

P. Zhang et al.

Table 1. Tree-ring sampling sites and summary statistics of the MXD data.

Sampling sites	Elev	TS	NS	MTA	AMXD	MS	AC1
Furuberget 1	650	873–1112	3	156	0.74	0.118	0.556
		1189–2005	104	168	0.69	0.122	0.571
Furuberget 2 (G11)	650	1497–2008	35	193	0.64	0.133	0.457
Håckervalen-top	750	783–1265	30	130	0.66	0.125	0.415
		1276–1520	24	113	0.60	0.134	0.449
Håckervalen	650	1778–2011	5	213	0.71	0.165	0.314
Lilla-Rörtjärnen*	560	952–1182	13	90	0.67	0.122	0.572
		1290–1668	9	147	0.63	0.122	0.655
		1750–1861	1	112	–	–	–
Öster Helgtjärnen*	646	929–1093	6	121	0.62	0.124	0.715
		1119–1333	3	104	0.72	0.122	0.625
		1336–1402	1	67	–	–	–
		1446–1568	2	110	0.76	0.106	0.676
Jens Perstjärnen*	700	1196–1382	2	153	0.62	0.133	0.753
Historical buildings	< 500	1107–1291	15	158	0.84	0.082	0.676
(Jämtland, Sweden)		1316–1827	118	161	0.79	0.089	0.576

Elev: source elevation (m a.s.l); TS: time span (CE); NS: number of samples; MTA: mean tree age (year); AMXD: average MXD ($g\,cm^{-3}$); MS: mean sensitivity; AC1: first-order autocorrelation; * means that the sampling site is a lake. Some of the "mean tree ages" are less than 100 years, because the MXD measurement is only a part of a tree-ring width measurement which is much longer. The cutting of the samples is due to that some parts of the samples were too rotten for MXD to be measured.

CPD
11, 489–519, 2015

1200 years of warm-season temperature variability

P. Zhang et al.

Table 2. Calibration and verification statistics of the warm-season temperature reconstruction.

MXD RSFi chronology			
Calibration period	1890–1950	1951–2011	1890–2011
Correlation, R	0.82[a]	0.67[a]	0.77[a]
Explained variance, R^2	0.67	0.46	0.59
No. of observations	61	61	122
Verification period	1951–2011	1890–1950	–
Explained variance, R^2	0.46	0.67	–
RE[b]	0.55	0.71	–
CE[b]	0.44	0.65	–

[a] the correlation is significant at $p < 0.01$ significance level; [b] RE means reduction of error; CE means coefficient of efficiency.

CPD
11, 489–519, 2015

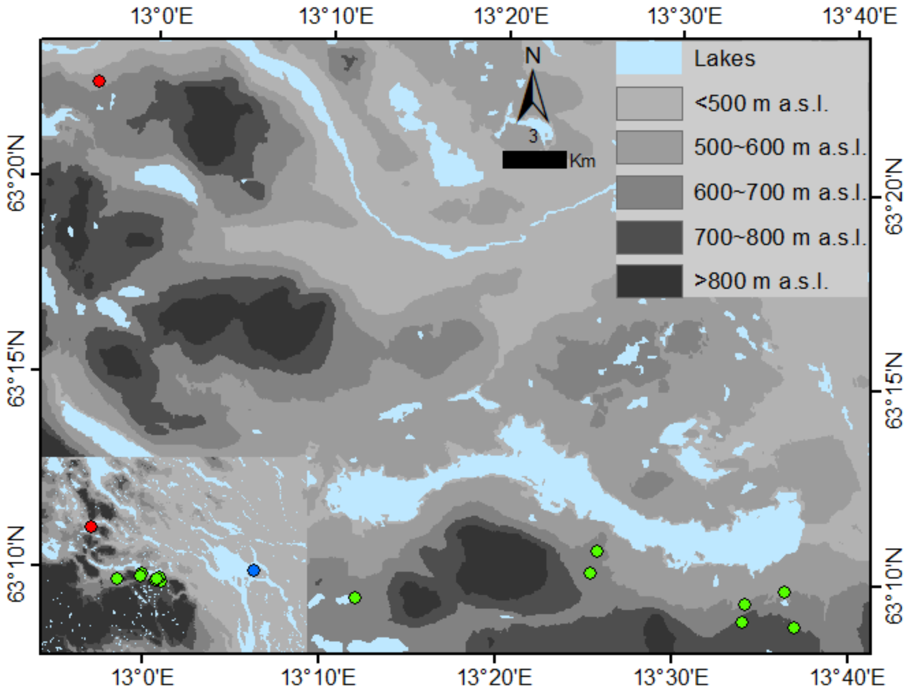

Figure 1. Map showing the locations of tree-ring sampling sites (green dots), except for historical samples, and Duved (red dot) and Östersund (blue dot) meterological station.

CPD
11, 489–519, 2015

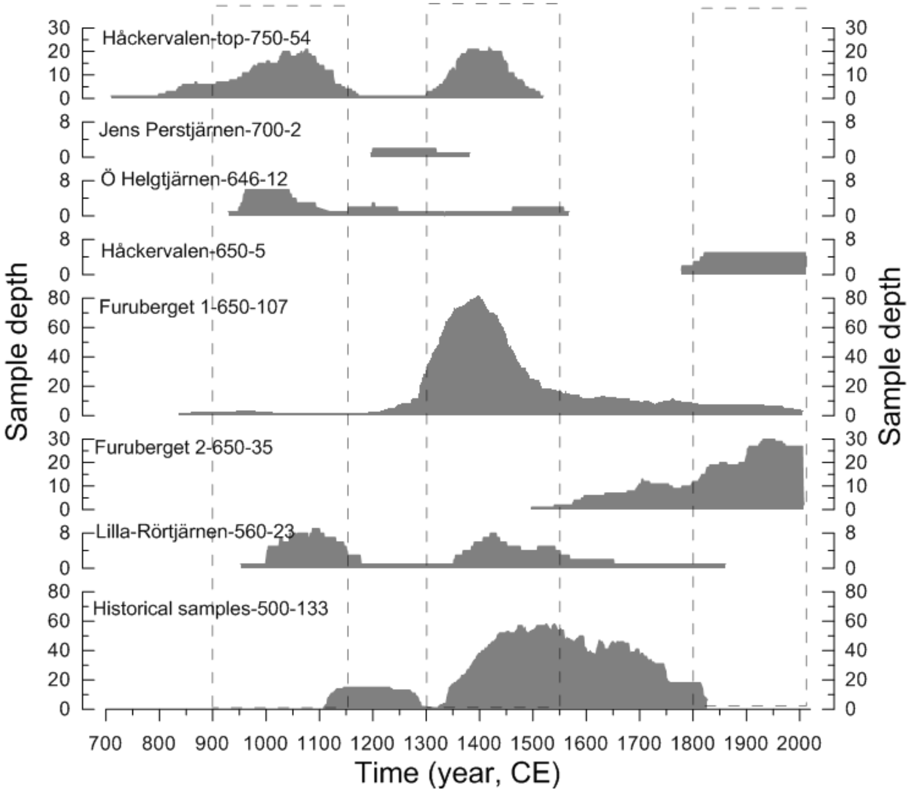

Figure 2. Sample replication and time span in each site/group. The site/group names, elevations and the number of samples were given on the upper left corner of each subplot. Dashed line frames mark three common periods with most of the samples.

CPD
11, 489–519, 2015

1200 years of warm-season temperature variability

P. Zhang et al.

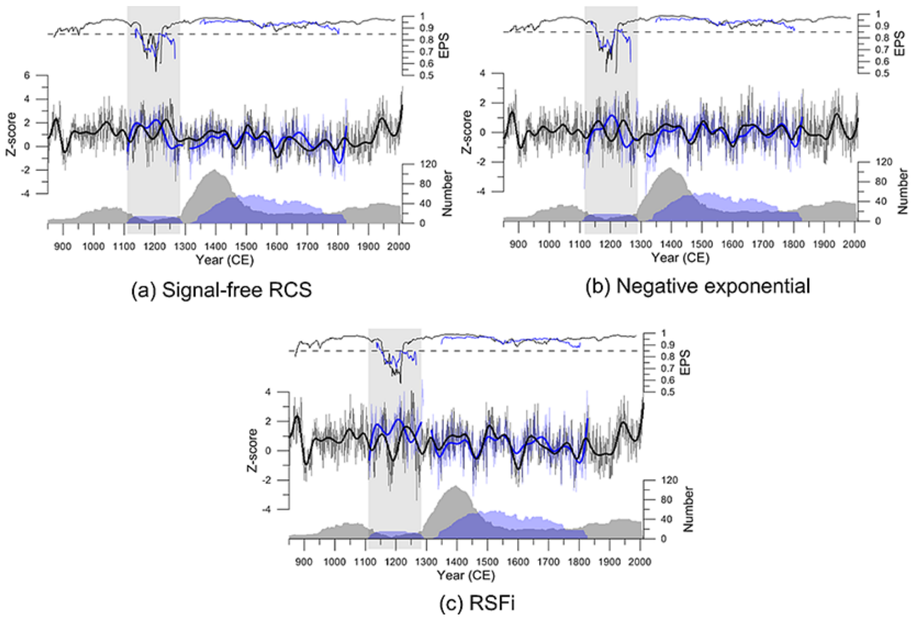

Figure 3. Comparison of the z scored (based on 1700–1800) interannual (thin curves in the middle subplot) and multi-decadal (50 year spline) (bold curves in the middle subplot) variability of the historical (blue) and "in-situ" sample based (black) chronologies after **(a)** signal-free RCS standardisation (smoothed by age-dependent spline), **(b)** negative exponential curve standardisation and **(c)** RSFi standardisation. Sample replication and EPS information was given in the lower and upper subplot. The low EPS time period around 12th century was marked by dark background.

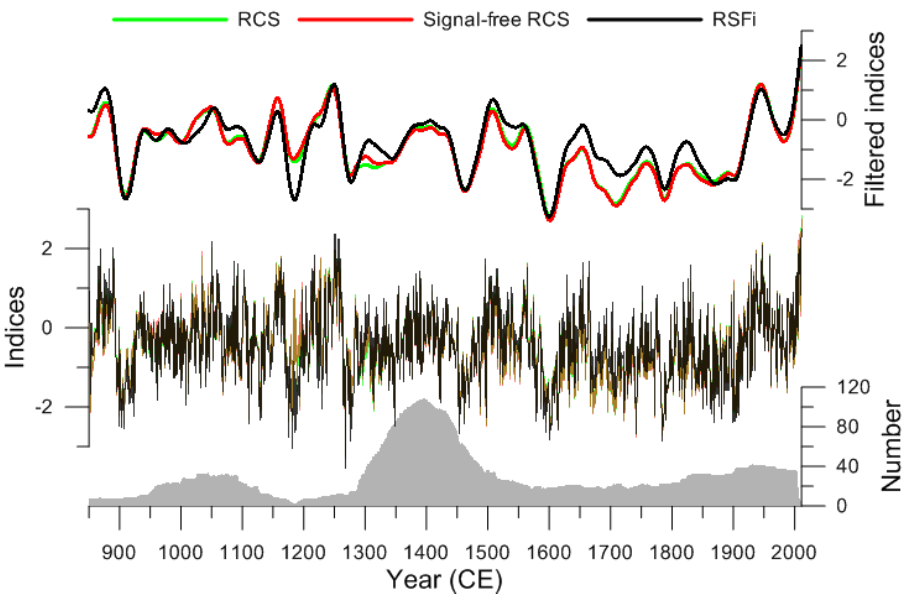

Figure 4. Comparison of the interannual (thin curves in the middle subplot) and multi-decadal (50 year spline) (bold curves in the upper subplot) variability in the mean-adjusted 238 field-sample based chronologies based on RCS standardisation (smoothed by hugershoff function) (green curves), signal-free RCS standardisation (smoothed by age-dependent spline) (red curves) and RSFi standardisation (black curves). Sample replication was given in the lower subplot.

CPD
11, 489–519, 2015

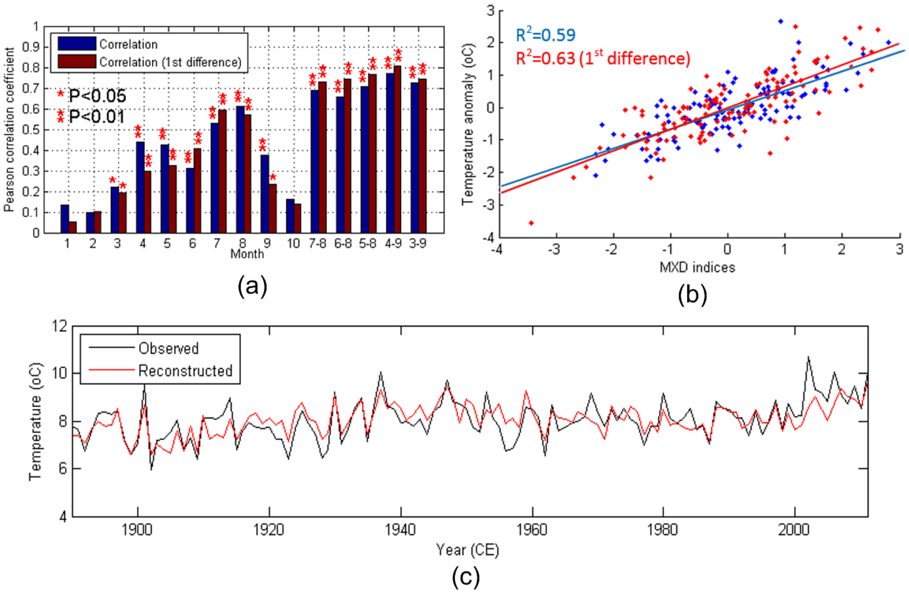

Figure 5. (a) Correlation between the mean-adjusted MXD data, standardised with RSFi method, and monthly mean temperature over the period of 1890–2011 CE. Correlations are given from January to October of the growth year and July–August, June–August, May–August April–September (warm season) and March–September average; **(b)** Linear relationship between MXD data and warm-season temperature (anomaly relative to 1961–1990 mean (blue) and 1st difference (red)); **(c)** comparison of reconstructed warm-season temperature (red) with observed Duved warm-season temperature (black) for the period of 1890–2011 CE.

CPD
11, 489–519, 2015

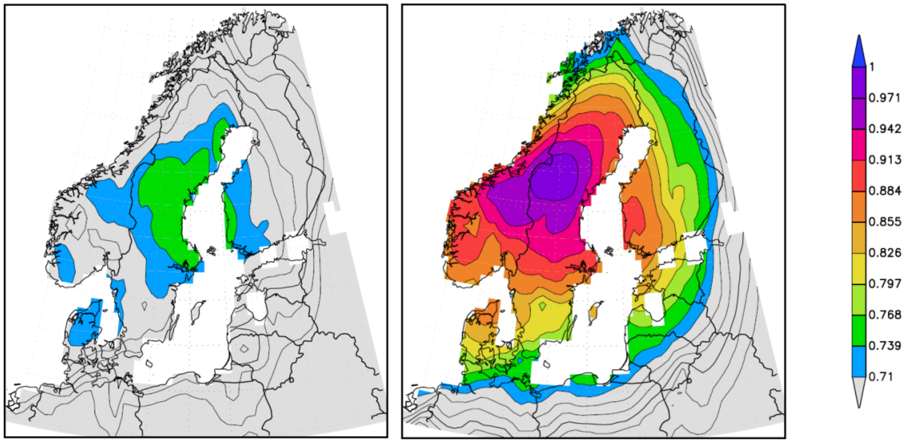

(a) (b)

Figure 6. Field correlations of the reconstructed warm-season temperature from **(a)** the new chronology in this study and **(b)** observed Duved warm-season temperature with the gridded warm-season temperature from CRU TS3.22 0.5×0.5 dataset during the period of 1901–2011 CE. Grey areas outside the $r = 0.71$ isoline represent the correlations at $p < 0.001$ significance level. Color bars represent the magnitude of the correlations.

CPD
11, 489–519, 2015

1200 years of warm-season temperature variability

P. Zhang et al.

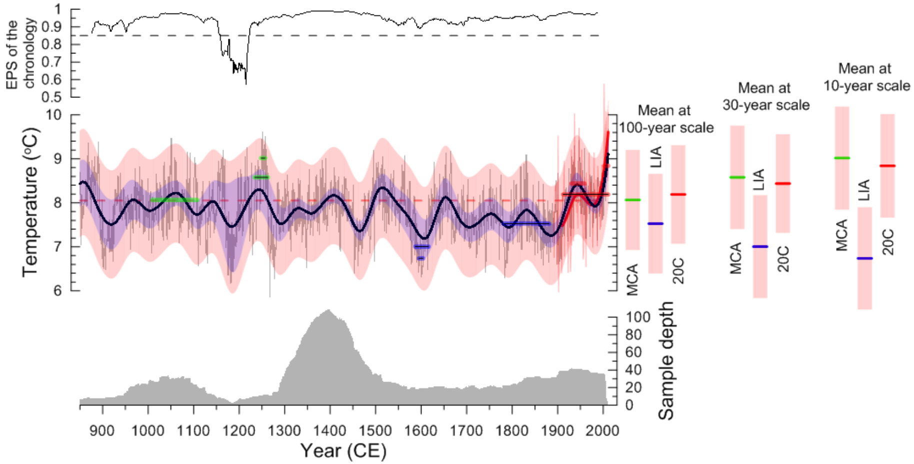

Figure 7. Annual (gray) and 80 year spline filtered (bold black) warm-season temperature variability over the period of 850–2011 CE inferred from the new chronology in this study. Purple and pink shading indicate the chronology uncertainty and the total uncertainty of the reconstruction (including chronology uncertainty and reconstruction uncertainty), as expressed as the 2× standard error in their upper and lower limitations. The gray shading and the thin black curve indicate the sample depth and EPS values (with the dashed line show the threshold of 0.85) of the chronology. Observed annual and 80 year spline filtered warm-season temperature is shown by the thin red curve and the bold curve, with the red dashed line indicating the 1961–1990 mean. The short lines in the right part of the panel mark the mean temperature levels of the warmest 100, 30 and 10 years in MCA (10th–13th century, Grove and Switsur, 1994) (green) and 20th century (red), and the coldest 100, 30 and 10 years in the LIA (14th–19th century, Grove, 2001) (blue). The time spans are marked on the corresponding positions on the temperature curve. The coloured short lines with thin solid black line in the centre mark the time spans of the warmest and coldest 100, 30 and 10 years during the past 1200 years.

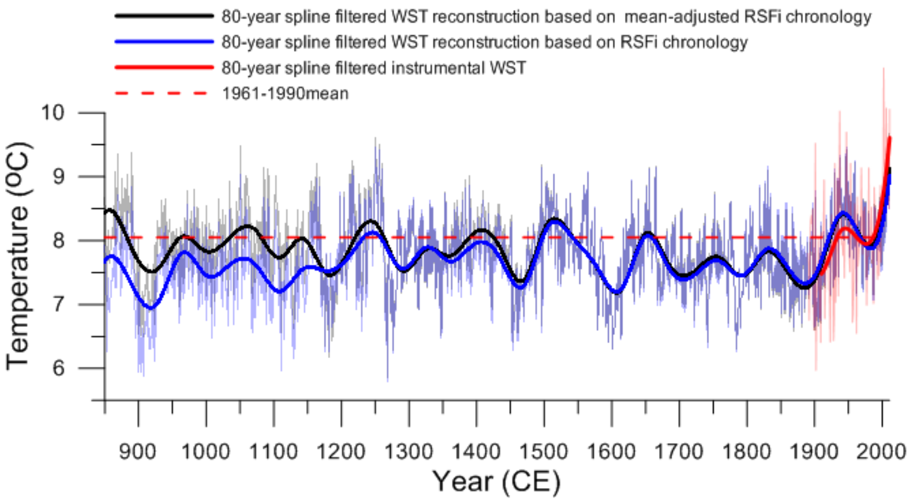

Figure 8. Comparison of the reconstructed warm-season temperature based on the mean-adjusted MXD samples (black) and the unadjusted MXD samples (blue). Red curves show the observed warm-season temperature variability. Light curves indicate the interannual variability, and the bold curves show the variability smoothed by 80 year spline filter. Dash line shows the observed 1961–1990 mean warm-season temperature.

CPD
11, 489–519, 2015

1200 years of warm-season temperature variability

P. Zhang et al.

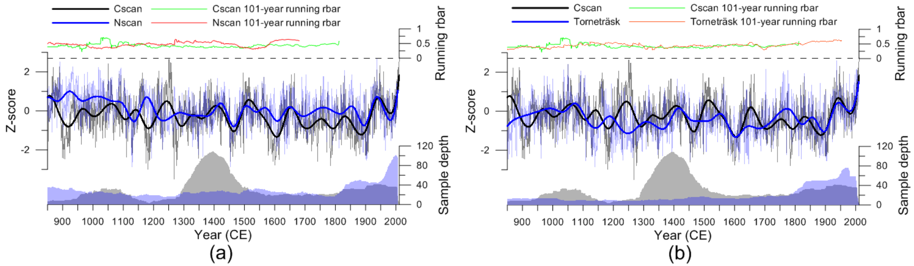

Figure 9. Comparison of annual variation of the *z* scored (based on 1890–2006) C-Scan (thin black curve) with **(a)** N-Scan (Esper et al., 2012) reconstruction (thin blue curve), and **(b)** Torneträsk (Melvin et al., 2013) reconstruction (thin blue curve). Bold black and blue curves show the variability after 80 year spline filtering. The sample depths (Number of trees) of the two chronologies are marked by the black (C-Scan) and blue (N-Scan) shadings. The green/orange line indicates 101 year running rbar of C-Scan and N-Scan chronologies. The dashed line is marked as 0 level. N-Scan data is downloaded from National Climatic Data Center, US National Oceanic and Atmospheric Administration (NOAA, http://www.ncdc.noaa.gov/paleo/primer_proxy.html) (ONLINE RESOURCE: http://www.ncdc.noaa.gov/paleo/study/16975).

Discussion Paper | Discussion Paper | Discussion Paper | Discussion Paper |

CPD

11, 489–519, 2015

1200 years of warm-season temperature variability

P. Zhang et al.